Electronic Supplementary Material (ESI) for Journal of Materials Chemistry A.

Supplementary information for

Garnet-based solid lithium metal batteries with ultralong lifespan enabled by solvent-free trifluoroacetic acid-induced interfacial engineering

Xia Hu[1], Yao Wang[1], Weiqian Guo[1], Yao Tian[1], Xiang Zhang[1], Feiyu Kang[1], Dong Zhou[1 *], Baohua Li[1 *]

1. Tsinghua Shenzhen International Graduate School, Tsinghua University, Shenzhen 518055, China.

* Corresponding author.

Email: zhou.d@sz.tsinghua.edu.cn;

libh@sz.tsinghua.edu.cn

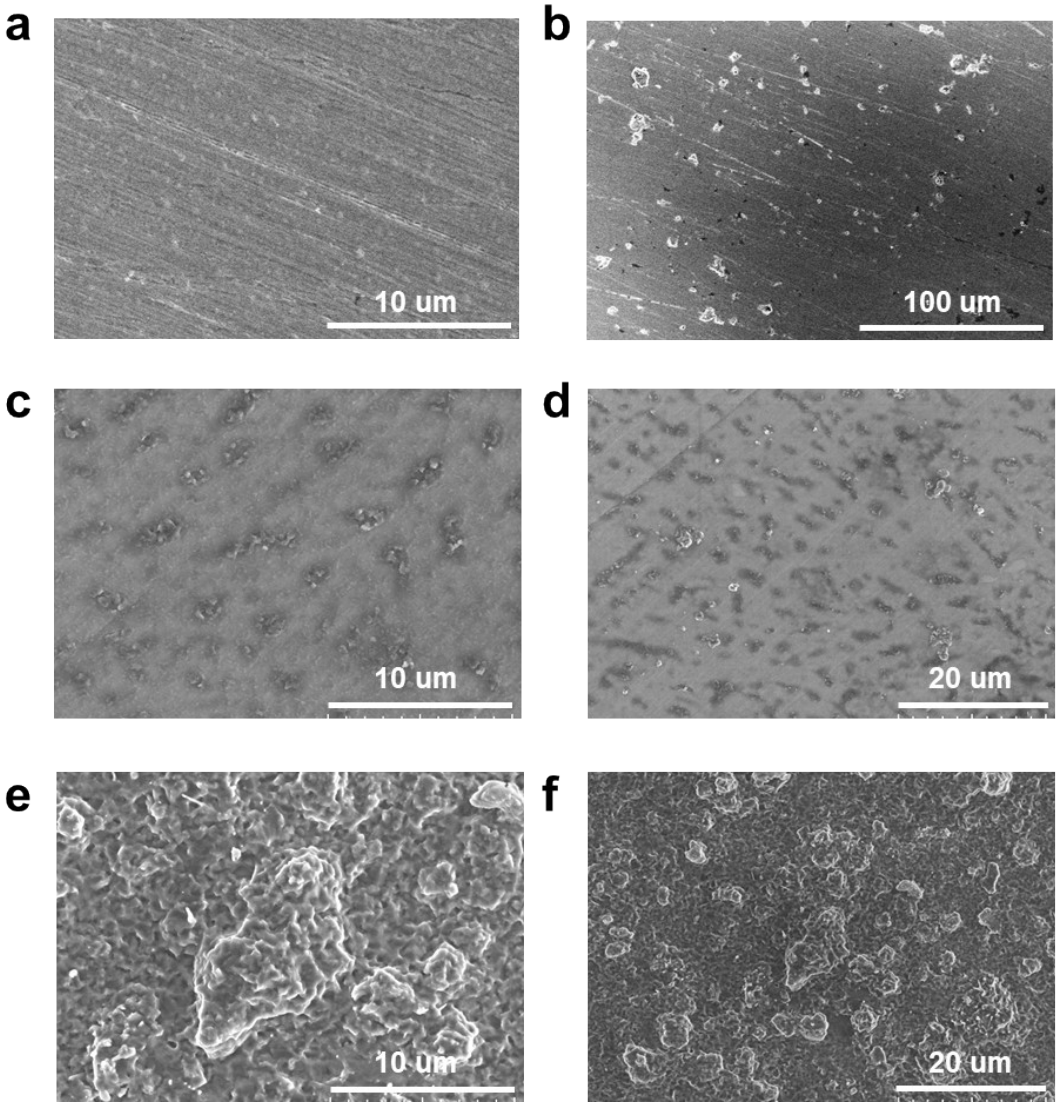

Supplementary Fig. 1 Top-view FE-SEM images of **a, b** bare LLZTO pellets, **c, d** LLZTO-1D pellets (exposed to humid air for one day) and **e, f** LLZTO-Air pellets (exposed to humid air for two days).

The FE-SEM images in Fig. S1 (Supporting Information) shows that with the increase of exposure time in humid air, the contaminant layer on the SSE surface becomes thicker, demonstrating its poor chemical stability with humid air.

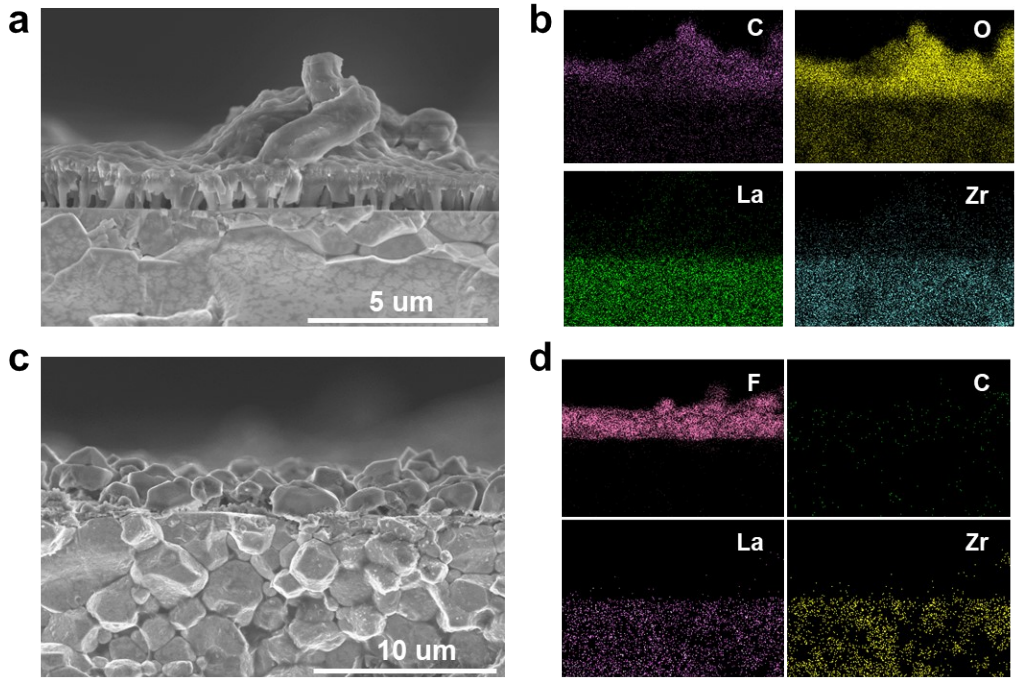

Supplementary Fig. 2 Cross-sectional FE-SEM images of **a** LLZTO-Air pellets and **b** its corresponding elemental mappings for C, O, La, Zr, **c** LLZTO-F pellets and **d** its corresponding elemental mappings for F, C, La, Zr.

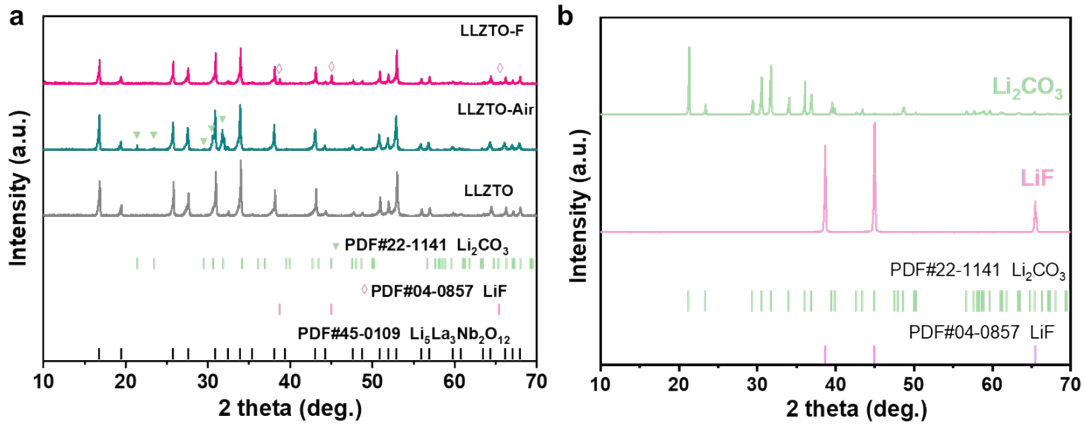

Supplementary Fig. 3 XRD patterns of **a** bare LLZTO, LLZTO-Air and LLZTO-F pellets, and **b** Li_2CO_3 and LiF.

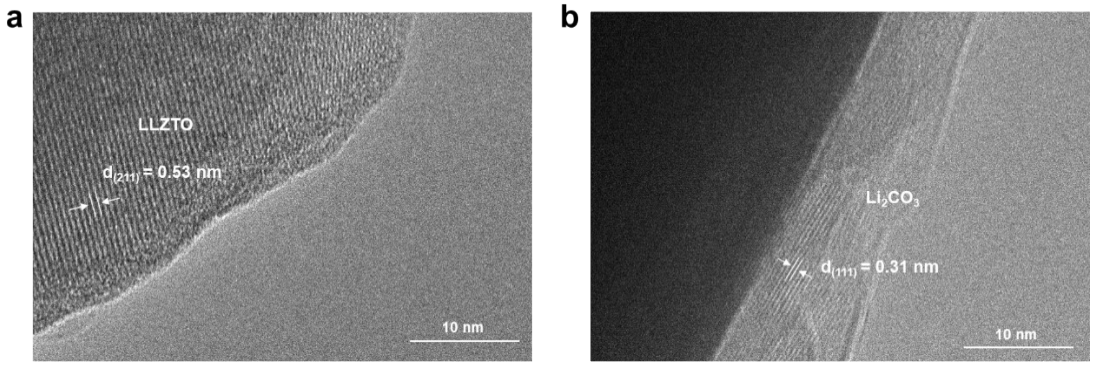

Supplementary Fig. 4 Cryo-TEM images of **a** bare LLZTO powder and **b** LLZTO-Air powder**.**

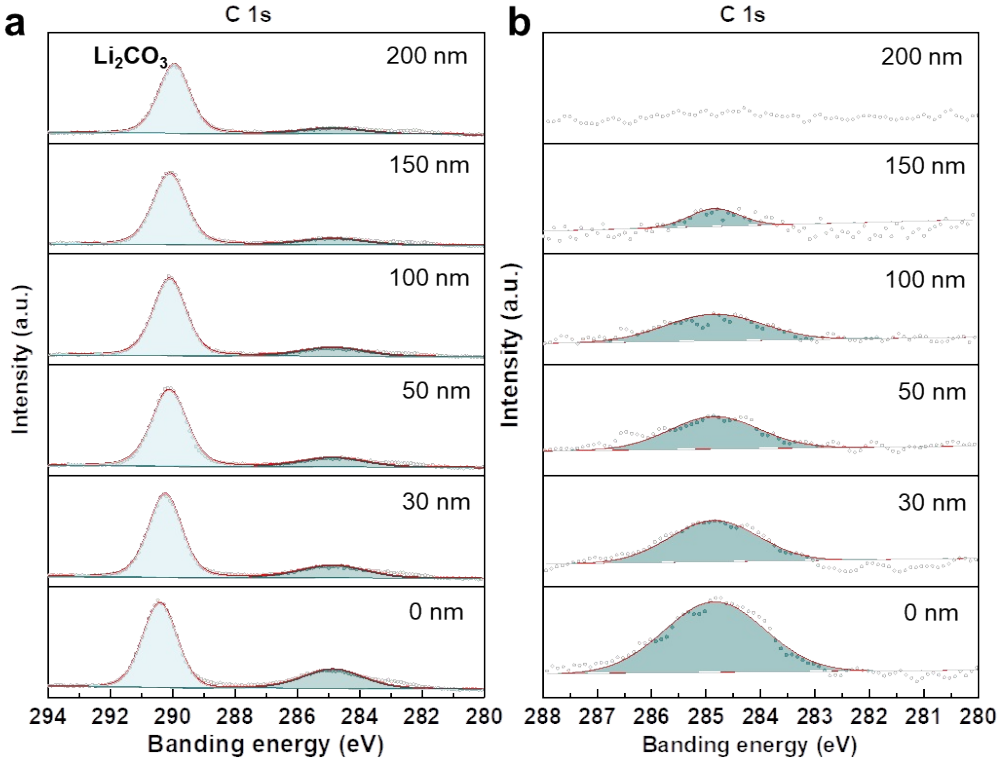

Supplementary Fig. 5 XPS depth profiles of the C 1s high-resolution spectrum of **a** LLZTO-Air and **b** LLZTO-F.

The strong Li_2CO_3 signal at 290.3 eV is attributed to the reaction of LLZTO with H_2O and CO_2 in the air. The peak in C 1 s spectra at 284.8 eV is revealed attributed to adventitious carbon[1,2].

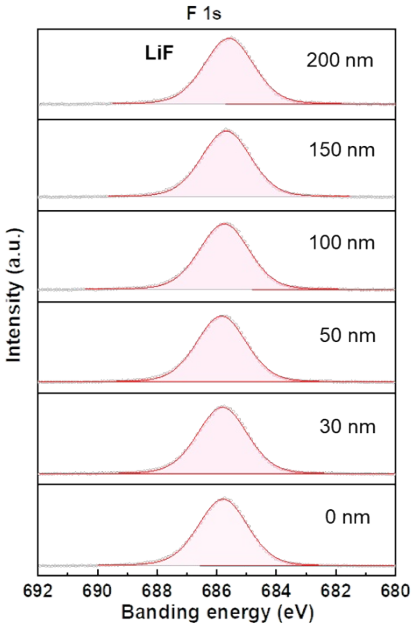

Supplementary Fig. 6 XPS depth profiles of the F 1s high-resolution spectrum of LLZTO-F. The distinct peak corresponding to the characteristic absorption peak of LiF at 685.8 eV can be observed.

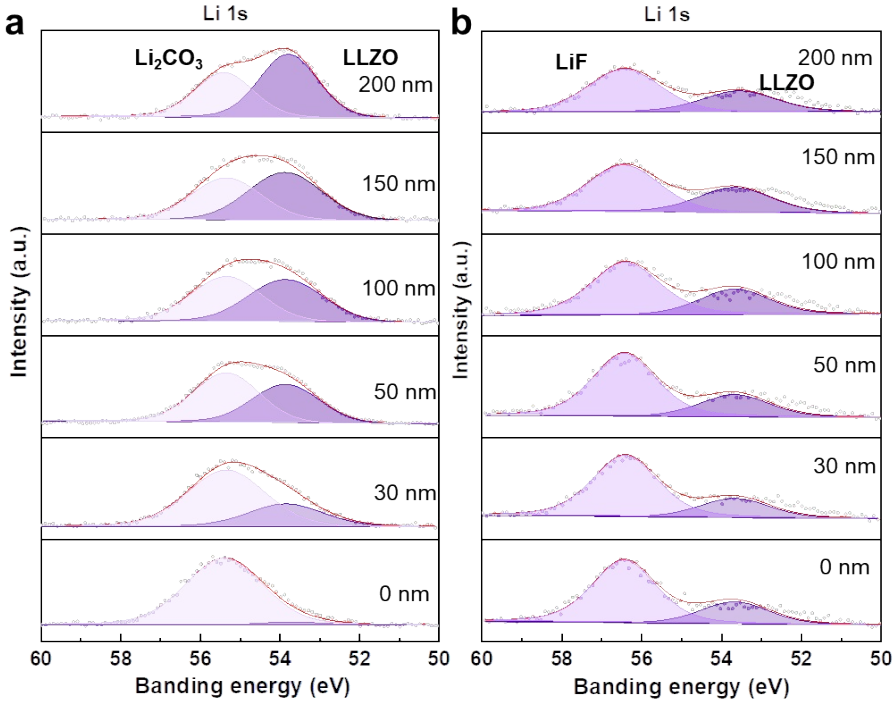

Supplementary Fig. 7 XPS depth profiles of the Li 1s high-resolution spectrum of **a** LLZTO-Air and **b** LLZTO-F.

For LLZTO-Air, the characteristic absorption peaks of LLZTO and Li_2CO_3 at 53.7 eV and 55.4 eV can be observed, respectively. In comparison, for LLZTO-F, the signal of Li_2CO_3 disappears, and the characteristic absorption peak of LiF at 56.4 eV can be detected [3].

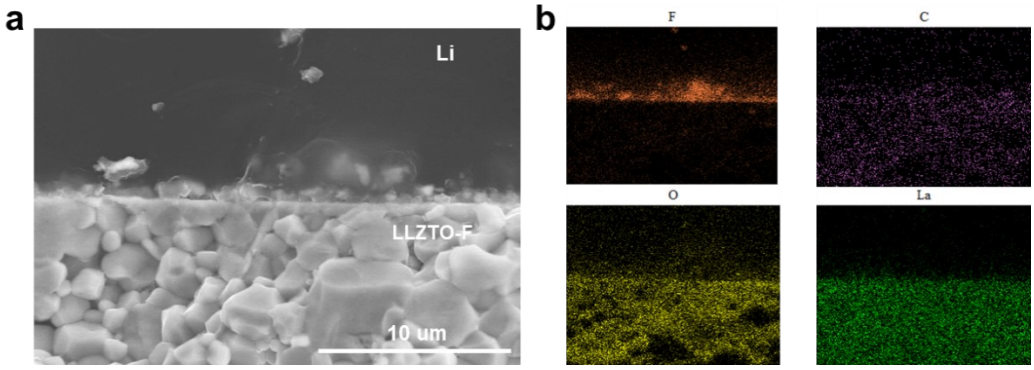

Supplementary Fig. 8 Cross section SEM images of a LLZTO-F pellets and **b** its corresponding elemental mappings for F, C, O, La.

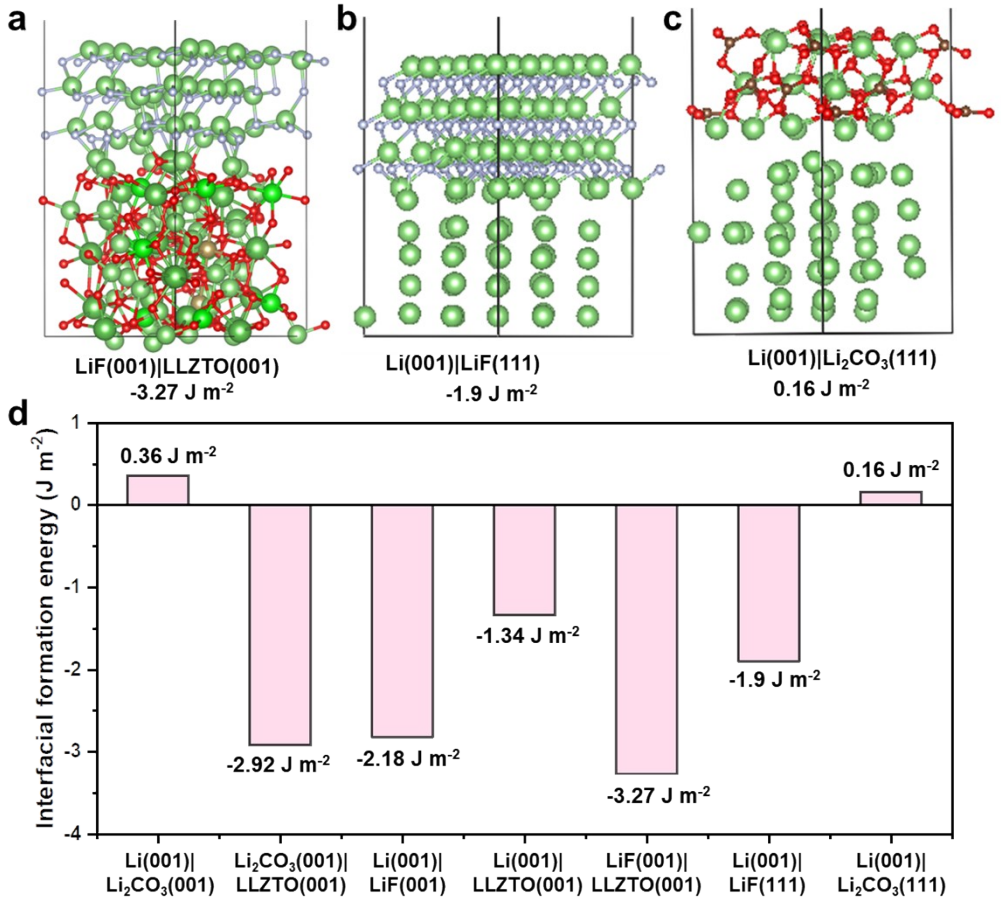

Supplementary Fig. 9 DFT calculations of the interfacial formation energies of the **a** LiF(001)|LLZTO(001), **b** Li(001)|LiF(111) and **c** Li(001)|Li_2CO_3(111), respectively. **d** Summary of calculation results of calculated interfacial formation energies indicating that the LiF layer largely improves the chemical bonding between Li and LLZTO.

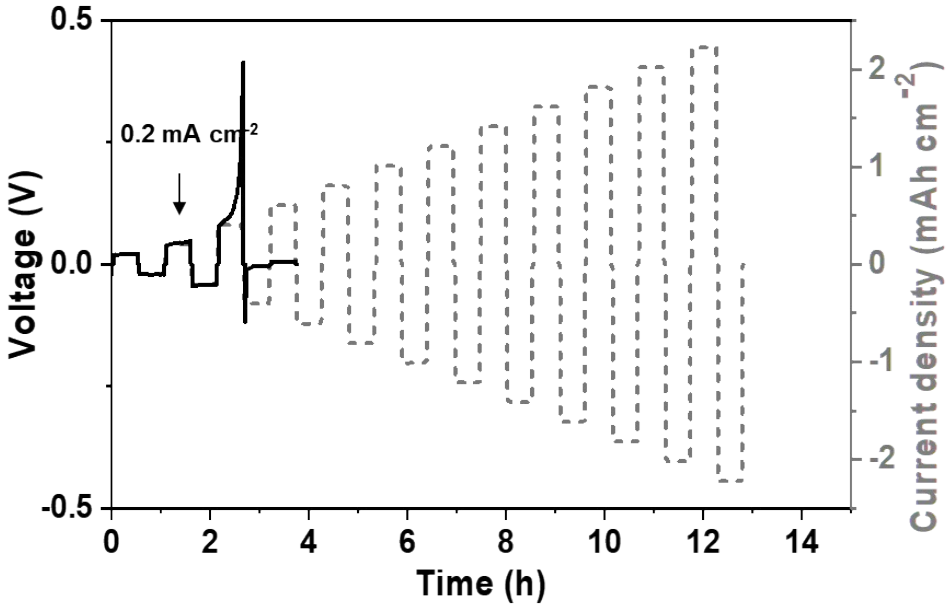

Supplementary Fig. 10 CCD curves of Li|bare-LLZTO|Li symmetric cells.

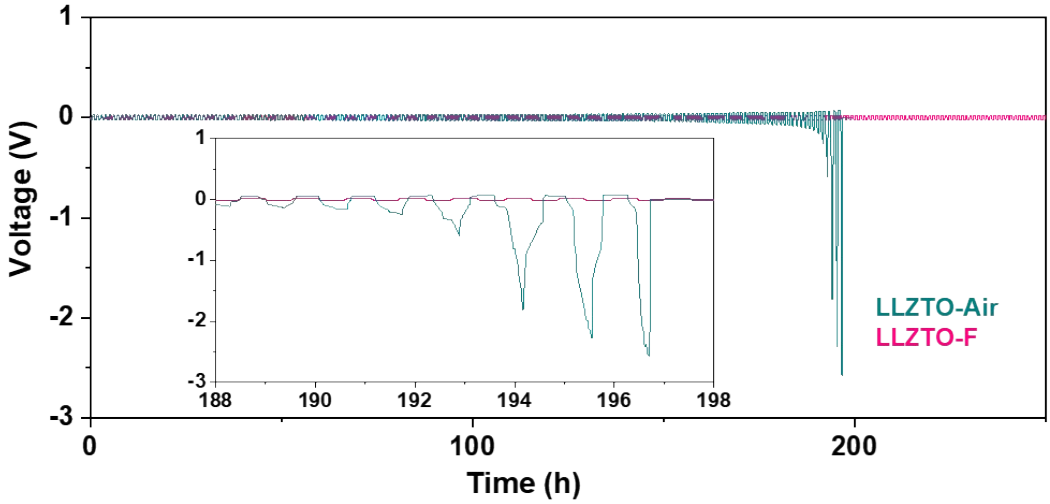

Supplementary Fig. 11 Enlarged voltage profiles of Li|LLZTO-Air|Li and Li|LLZTO-F|Li symmetrical cells for 0-250 h cycled at 0.1 mA cm^{-2} with a capacity of 0.05 mAh cm^{-2}, insets show voltage profiles for 188-198 h.

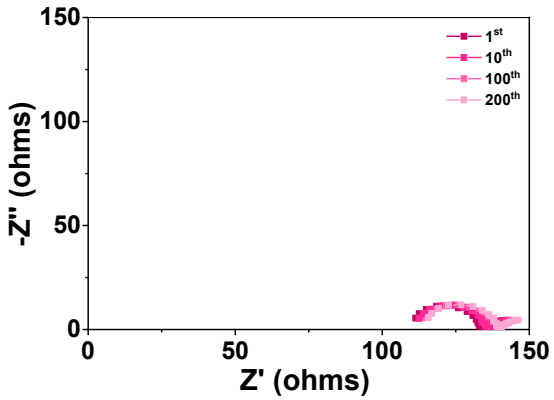

Supplementary Fig. 12 EIS spectra of Li|LLZTO-F|Li symmetrical cells after cycling.

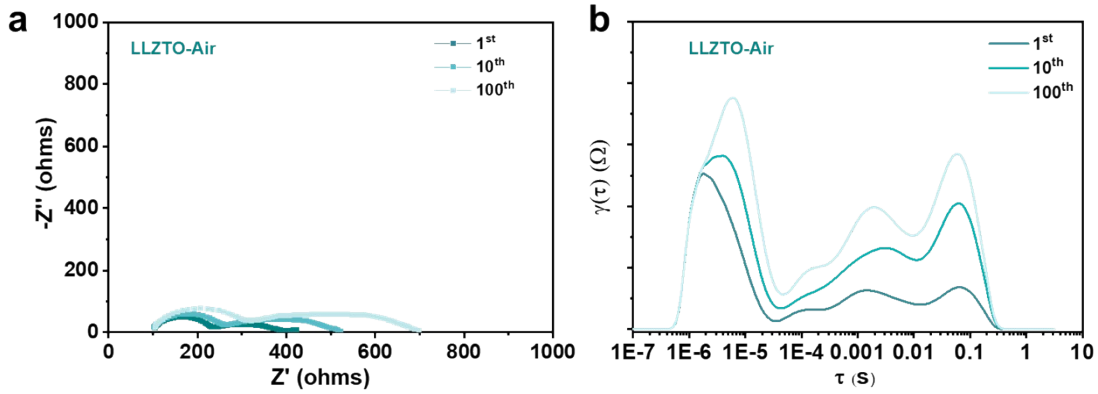

Supplementary Fig. 13 EIS spectra of **a** Li|LLZTO-Air|Li symmetrical cells and **b** the corresponding DRT profiles.

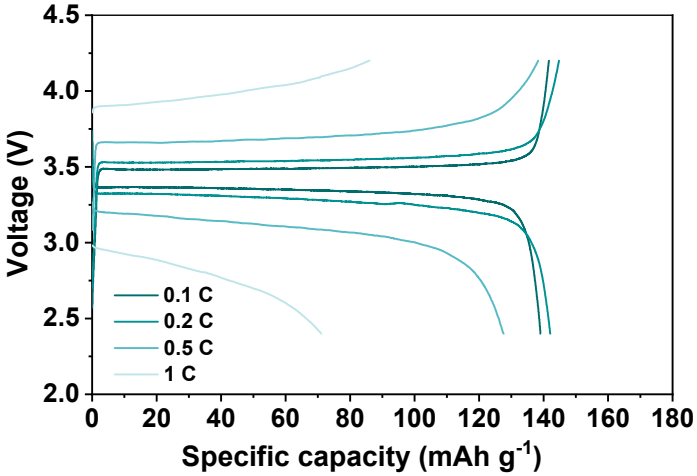

Supplementary Fig. 14 Charge/discharge profiles of Li|LLZTO-Air|LFP full cells at different rates at 25 °C.

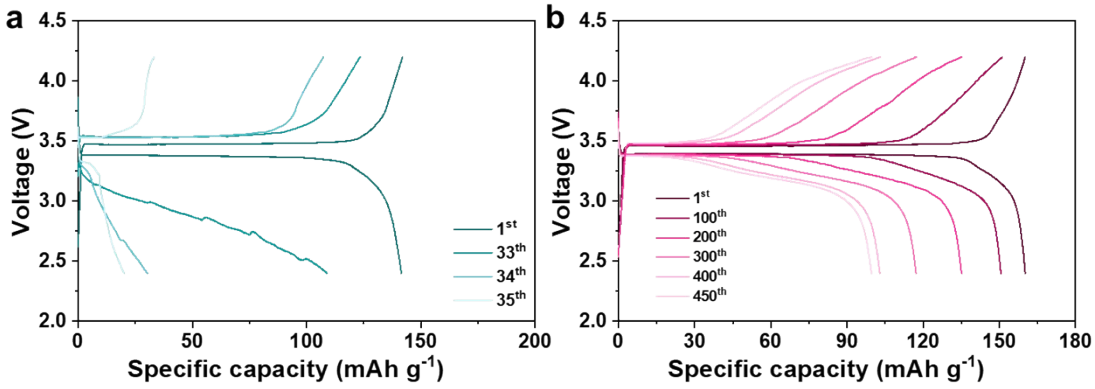

Supplementary Fig. 15 Charge/discharge profiles of **a** Li|LLZTO-Air|LFP full cell and **b** Li|LLZTO-F|LFP full cell during deferent cycles at 0.1 C at 25 °C.

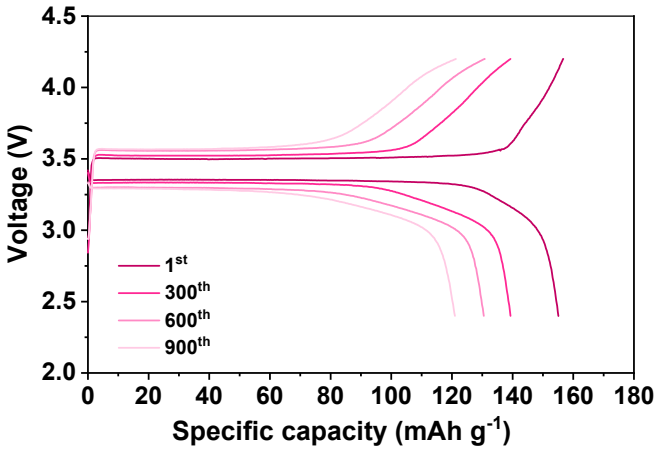

Supplementary Fig. 16 Charge/discharge profiles of Li|LLZTO-Air|LFP full cell during deferent cycles at 0.5 C at 25 °C.

Table S1. CCD and cycling stability of the reported Li||Li symmetrical cells and LFP||Li full cells using garnet SSEs with different interfacial layers.

SSE	interfacial layer	CCD (mA cm^{-2})	Stability (mA cm^{-2}@ mAh cm^{-2})/h	Rate/cycle number/capacity retention of LFP||Li cell	Ref.
$Li_{6.4}$ $La_3Zr_{1.4}Ta_{0.6}O_{12}$	CA	0.38	0.25@0.125/350	/	1
$Li_{6.4}La_3Zr_{1.4}Ta_{0.6}O_{12}$	H_3BO_3+HF	2	0.5@0.25/1200	1 C/200/ >90%, 60°C	2
$Li_{6.4}La_3Zr_{1.4}Ta_{0.6}O_{12}$	SiO_2	1.2	0.1@.1/1000 0.3@0.3/100	0.05 C/80/95%	4
$Li_{6.4}La_3Zr_{1.4}Ta_{0.6}O_{12}$	$NH_4H_2PO_4$	0.8	0.1@0.05/1000	/	5
Ta-substituted $Li_7La_3Zr_2O_{12}$	HCl+LiF	1.8	0.5@0.25/1000	0.25 C/30/ >95%	6
$Li_{6.4}La_3Zr_{1.4}Ta_{0.6}O_{12}$	HCl	/	0.2@0.1/700	0.1 C/150/ 82.1%	7
$Li_{6.4}La_3Zr_{1.4}Ta_{0.6}O_{12}$	PAA	1.8	0.2@0.2/2500 0.5@0.25/400	1 C/500/92.3%, 60 °C	8
Ta-substituted $Li_7La_3Zr_2O_{12}$	H_3PO_4	1.1	0.1@0.05/1600 0.5@0.25/450	~0.13 C/100/ 100%	9
$Li_{6.4}La_3Zr_{1.4}Ta_{0.6}O_{12}$	NH_4F	1.4	0.3@0.15/600 0.4@0.2/250 0.5@0.25/220	0.2C/50/>90%	10
$Li_{6.4}La_3Zr_{1.4}Ta_{0.6}O_{12}$	$LiPO_2F$	1.2	0.6@0.3/1600 0.8@0.4/180	/	11
$Li_{6.4}La_3Zr_{1.4}Ta_{0.6}O_{12}$	$LiPF_6$	1.1	0.2@0.2/700 60°C 0.5@0.2/250 60°C	0.5 C/190/ 93.6%, 60°C	12
$Li_{6.4}La_3Zr_{1.4}Ta_{0.6}O_{12}$	**TFA**	**2.0**	**0.1@0.05/10000 0.5@0.25/1200**	**0.5 C/900/ 78.0%**	**This work**

References

1 Gao, J., Guo, W., Yin, Y., Sun, Z., Zhao, B., Shen, F. & Han, X. *Mater. Lett.*, 2020, **280**, 128543.

2 Cai, M., Jin, J., Xiu, T., Song, Z., Badding, M. E. & Wen, Z. *Energy Storage Mater.*, 2022, **47**, 61-69.

3 Guo, C., Shen, Y., Mao, P., Liao, K., Du, M., Ran, R., Zhou, W. & Shao, Z. *Adv. Funct. Mater.*, 2022, **33**, 2213443.

4 Zhang, J., Wang, C., Zheng, M., Ye, M., Zhai, H., Li, J., Tan, G., Tang, X. & Sun, X. *Nano Energy*, 2022, **102**.

5 Bi, Z., Sun, Q., Jia, M., Zuo, M., Zhao, N. & Guo, X. *Adv. Funct. Mater.*, 2022, **32**, 2208751.

6 Ruan, Y., Lu, Y., Li, Y., Zheng, C., Su, J., Jin, J., Xiu, T., Song, Z., Badding, M. E. & Wen, Z. *Adv. Funct. Mater.*, 2020, **31**, 2007815.

7 Huo, H., Chen, Y., Zhao, N., Lin, X., Luo, J., Yang, X., Liu, Y., Guo, X. & Sun, X. *Nano Energy*, 2019, **61**, 119-125.

8 Guo, C., Shen, Y., Mao, P., Liao, K., Du, M., Ran, R., Zhou, W. & Shao, Z. *Adv. Funct. Mater.*, 2022, **33**.

9 Ruan, Y., Lu, Y., Huang, X., Su, J., Sun, C., Jin, J. & Wen, Z. *J. Mater. Chem. A*, 2019, **7**, 14565-14574.

10 D., H., Wan–Ping Chen, Min Fan, Wen–Peng Wang, Le Yu, Shuang-Jie Tan, Xiang Chen, Qiang Zhang, Sen Xin, Li–Jun Wan & Guo, Y. G. *Angew. Chem. Int. Ed.*, 2020, **59**, 12069-12075.

11 Yang, X., Tang, S., Zheng, C., Ren, F., Huang, Y., Fei, X., Yang, W., Pan, S., Gong, Z. & Yang, Y. *Adv. Funct. Mater.*, 2022, **33**, 2209120.

12 Chen, N., Gui, B., Yang, B., Deng, C., Liang, Y., Zhang, F., Li, B., Sun, W., Wu, F. & Chen, R. *Small*, 2023, 2305576.